



# CT-based radiomics features analysis for predicting the risk of anterior mediastinal lesions

He Sui<sup>1</sup>, Lin Liu<sup>1</sup>, Xuejia Li<sup>1</sup>, Panli Zuo<sup>2</sup>, Jingjing Cui<sup>2</sup>, Zhanhao Mo<sup>1</sup>

<sup>1</sup>Department of Radiology, China-Japan Union Hospital of Jilin University, Changchun 130033, China; <sup>2</sup>Huiying Medical Technology Co., Ltd., Beijing 100192, China

**Contributions:** (I) Conception and design: Z Mo; (II) Administrative support: L Liu; (III) Provision of study materials or patients: H Sui; (IV) Collection and assembly of data: H Sui, X Li; (V) Data analysis and interpretation: P Zuo, J Cui; (VI) Manuscript writing: All authors; (VII) Final approval of manuscript: All authors.

**Correspondence to:** Zhanhao Mo. Department of Radiology, China-Japan Union Hospital of Jilin University, Changchun 130033, China. Email: mozhanhao@jlu.edu.cn.

**Background:** To retrospectively validate CT-based radiomics features for predicting the risk of anterior mediastinal lesions.

**Methods:** A retrospective study was performed through February 2013 to March 2018 on 298 patients who had pathologically confirmed anterior mediastinal lesions. The patients all underwent CT scans before their treatment, including 130 unenhanced computed tomography (UECT) and 168 contrast-enhanced CT (CECT) scans. The lesion areas were delineated, and a total of 1,029 radiomics features were extracted. The least absolute shrinkage and selection operator (Lasso) algorithm method was used to select the radiomics features significantly associated with discrimination of high-risk from low-risk lesions in the anterior mediastinum. Then, 8-fold and 3-fold cross-validation logistic regression (LR) models were taken as the feature selection classifiers to build the radiomics models for UECT and CECT scan respectively. The predictive performance of the radiomics features was evaluated based on the receiver operating characteristics (ROC) curve.

**Results:** Each of the two radiomics classifiers included the optimal 12 radiomic features. In terms of the area under ROC curve, using the radiomics model in discriminating high-risk lesions from the low-risks, CECT images accounted for 74.1% with a sensitivity of 66.67% and specificity of 64.81%. Meanwhile, UECT images were 84.2% with a sensitivity of 71.43% and specificity of 74.07%.

**Conclusions:** The association of the two proposed CT-based radiomics features with the discrimination of high and low-risk lesions in anterior mediastinum was confirmed, and the radiomics features of the UECT scan were proven to have better prediction performance than the CECT's in risk grading.

**Keywords:** Radiomics; histologic grade; unenhanced computed tomography (UECT); contrast-enhanced computed tomography (CECT); anterior mediastinum

Submitted Nov 24, 2018. Accepted for publication Apr 25, 2019.

doi: 10.21037/jtd.2019.05.32

**View this article at:** <http://dx.doi.org/10.21037/jtd.2019.05.32>

## Introduction

Due to the wide range of types involved in anterior mediastinal lesions, a differential diagnosis and risk evaluation bring continuous challenges to clinicians (1). Thymic epithelial tumors are the most primary neoplasms in the anterior mediastinum (2), and are histologically

divided by the World Health Organization (WHO) into type A, type AB, type B1, type B2, type B3, and type C (heterogeneous thymic carcinomas), based on the ratios of lymphocytes to epithelial cells and the morphology of epithelial cells (3-5). Also, there is a simplified classification that defines type A, AB, and B1 thymomas as low-risk and type B2 and B3 thymomas and type C as high-risk

lesions. This simplified risk classification is closely related to the patients' outcome and the prognosis according to the WHO classification. It is reported that high-risk thymic epithelial tumors have a much poorer prognosis and a higher recurrence rate when compared with low-risk thymic epithelial tumors (6). In addition to thymic epithelial tumors, some benign masses with good prognosis, such as hemangiomas and cysts, were classified as being low-risk or high-risk malignant masses like lymphoma, which are also commonly found in the anterior mediastinum. Accurate pre-treatment evaluation of risks on anterior mediastinal lesions has become crucial because of its impact on surgical planning and prognosis assessment (7). Hence, an effective and objective approach is urgently needed to estimate the clinical risk of anterior mediastinal masses before treatment.

Chest CT scans are the routine examination in delineating anterior mediastinal masses (8). However, there are no specific characteristics concerning the differential diagnosis of anterior mediastinal lesions (9). Recently, radiomics has aroused increasing attention, mainly due to its ability to extract large quantities of high-throughput imaging features, and transform medical images into mineable high-dimensional data. The subsequent quantitative analysis of these data can offer help in assessing the risk of lesions in the anterior mediastinum based on CT (10-12). Radiomics has been applied in the grading and staging of tumors, including those of lung cancers (13), renal carcinomas, breast carcinomas, and colorectal adenocarcinomas. It has also found use in assessing anterior mediastinal lesions, including in estimating thymic epithelial tumors' grading and staging (14), distinguishing solid and cyst masses (15), and identifying histological subtypes of thymic epithelial tumors (16). Nevertheless, only quantitative texture analysis (QTA), one branch of radiomics analyses, has been adopted.

This study aimed to build a CT-based radiomics model and validate its predictive ability on high-risk lesions from low-risk ones in the anterior mediastinum.

## Methods

### Patients

This retrospective study received the approval from the Institutional Review Board, and informed consent was obtained from all patients. A total of 298 patients from February 2013 to March 2018, including 130 for the unenhanced computed tomography (UECT) scan

(59 males and 71 females; age range, 17–86 years old; mean, 52.26±11.08 years old) and 168 for the contrast-enhanced CT (CECT) scan (72 males and 96 females; age range 18–86 years old; mean, 52±11.29 years old) affected by anterior mediastinal masses were retrospectively retrieved from the China-Japan Union Hospital and the Second Hospital of Jilin University. Patients were selected according to the following inclusion principles:

- (I) Histopathological diagnosis of anterior mediastinal lesions obtained by biopsy, mediastinoscopy, or surgery (*Table 1*);
- (II) Good quality UECT and CECT images with the same scan parameters for radiomics analysis;
- (III) No previous chemotherapy, radiation therapy, or biopsy.

Because teratomas have quite a specific performance on CT scan and can be easily distinguished by visual observation, we excluded teratomas from this analysis.

### CT images

UECT and CECT images were scanned by Toshiba Medical Systems CT scanners (Tochigi, Japan) and GE Healthcare CT scanner (Waukesha, WI). Automatic tube current modulation techniques were adopted with the tube voltage set at 120 kVp. The noise index of the SD was set as 11.6 and 13.0 for the GE and the Toshiba scanner respectively (80–100 mL) was injected at the speed of 2–3 mL/s, and the venous-phase CECT scan was then performed for 60 s. The UECT and CECT images were all reconstructed with a section thickness of 5 mm and an image slice matrix of 512×512.

### Lesion delineation and segmentation

All the UECT and CECT images were loaded into the RadCloud platform (Huiying Medical Technology Co., Ltd., Beijing, China). Volume of interests (VOIs) generally considered to be lesions were delineated on both UECT and venous-phase CECT images by a radiologist who had 3 years' clinical experience but was blinded to the clinical and histological information. Afterward, the VOIs were checked by a senior radiologist with more than 5 years of clinical experience, who decided on the lesions' borders when a discrepancy occurred (10) (*Figure 1*).

### Feature extraction

In total, 1,029 quantitative imaging features were extracted

**Table 1** Characteristics of patients in UECT and CECT scan

Diagnoses	Number	Gender		Age (years, mean $\pm$ SD)	Lesion volume (cm <sup>3</sup> )
		Male	Female		
<b>UECT</b>					
High-risk		23	33	54.29 $\pm$ 13.17	132.21 $\pm$ 229.18 (range: 1.00–1,111.44)
Thymic carcinoma	9				
Lymphoma	2				
WHO type B2 thymoma	14				
WHO type B3 thymoma	8				
Small cell carcinoma	1				
Seminoma	2				
Metastatic lymphoma node	3				
Adenocarcinoma	1				
Low-risk		36	38	51.42 $\pm$ 9.97	52.57 $\pm$ 96.08 (range: 0.42–558.76)
Thymic cyst	40				
Hemangioma	2				
Thymic hyperplasia	7				
Bronchogenic cyst	8				
Tuberculosis	1				
WHO type A thymoma	8				
WHO type AB thymoma	16				
WHO type B1 thymoma	8				
P		0.691		0.199	0.006
<b>CECT</b>					
High-risk		50	38	50.86 $\pm$ 12.93	128.85 $\pm$ 227.17 (range: 1.41–4,100.18)
Thymic carcinoma	8				
Lymphoma	8				
WHO type B2 thymoma	25				
WHO type B3 thymoma	16				
Small cell carcinoma	16				
Seminoma	2				
Metastatic lymphoma node	3				
Low-risk		32	58	53.11 $\pm$ 9.52	53.14 $\pm$ 96.45 (range: 1.55–5,388.80)
Thymic cyst	33				
Hemangioma	2				
Thymic hyperplasia	7				
Bronchogenic cyst	5				
Tuberculosis	1				
WHO type A thymoma	13				
WHO type AB thymoma	21				
WHO type B1 thymoma	8				
P		0.082		0.199	0.009

UECT, unenhanced computed tomography; CECT, contrast-enhanced computed tomography.

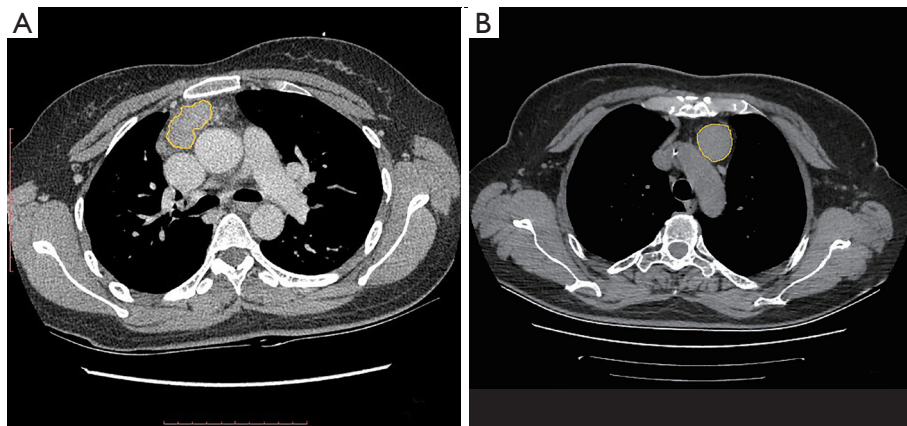


**Figure 1** Examples of anterior mediastinal lesion segmentation. (A) Venous-phase CECT images. A 56-year-old woman with thymic cyst; (B) UECT images. A 67-year-old woman with WHO type AB thymoma. UECT, unenhanced computed tomography; CECT, contrast-enhanced computed tomography.

from UECT and venous-phase CECT images with the RadCloud platform. They were classified into four groups. Group 1 covered the intensity features (including 19 descriptors) that quantitatively delineated the distribution of voxel intensities within the CT image through the basic metrics found in common. Group 2 (shape features) consisted of 15 three-dimensional (3D) features reflecting the shape and size of the target region. Texture features were divided into three types based on the calculations obtained from the grey level co-occurrence matrix, grey level size zone matrix, and grey level run length matrix. A total of 69 features were able to be quantified as regions with heterogeneity differences and were classified into Group 3 (texture features). The above three groups all extracted features from the VOIs of the original image.

Group 4 (higher-order features), with 966 features, included the intensity and texture features that were derived from the wavelet transformation and the filters of the original image. Furthermore, exponential, square, square root, logarithm, and wavelet (wavelet-LLL, wavelet-HHH, wavelet-HLL, wavelet-HHL, wavelet-LLH, wavelet-HLH, wavelet-LHL, wavelet-LHH) were derived from the original images that were used as filters.

#### ***Radiomics features selection and machine learning***

All statistical analyses were performed in Python (Version 2.7). We used Least absolute shrinkage and selection operator (Lasso) algorithm methods for the feature selection, in order to single out the optimal features. In this

process, we used 5- and 6-fold validation to find the best parameters with 3,000 iteration.

The cost function of LASSO method is:

$$L = \min_w \frac{1}{2n} \|Xw - y\|_2^2 + a \|w\|_1$$

$X$ : the matrix of radiomic features;  $y$ : the vector of the sample labels;  $n$ : the number of samples;  $w$ : the coefficient vector of the LASSO model;  $a \|w\|_1$ : the LASSO penalty with the constant  $a$  and the  $\ell_1$ -norm of coefficient vector  $\|w\|_1$ .

We used Logistic regression (LR) classifier with 8-fold validation on UECT selected features and 3-fold validation LR classifier on CECT selected features.

The cost function of LR as following:

$$Y = \min_{w,c} \frac{1}{2} w^T w + C \sum_{i=1}^n \log(\exp(-y_i(X_i^T w + c)) + 1)$$

$X$ : the matrix of radiomic features;  $y$ : the vector of the sample labels;  $w$ : the coefficient vector of the LR model;  $C$ : inverse of regularization strength.

#### ***Predictive performance of machine learning***

The receiver operating characteristics (ROC) curve analysis was employed to evaluate the prediction ability of the selected radiomics features. The optimal cutoff value was selected as the point when both the sensitivity and specificity were maximal. In the area under the curve (AUC), sensitivity and specificity were calculated in both the training and validation sets of UECT and CECT.

The workflow is shown in *Figure 2*.

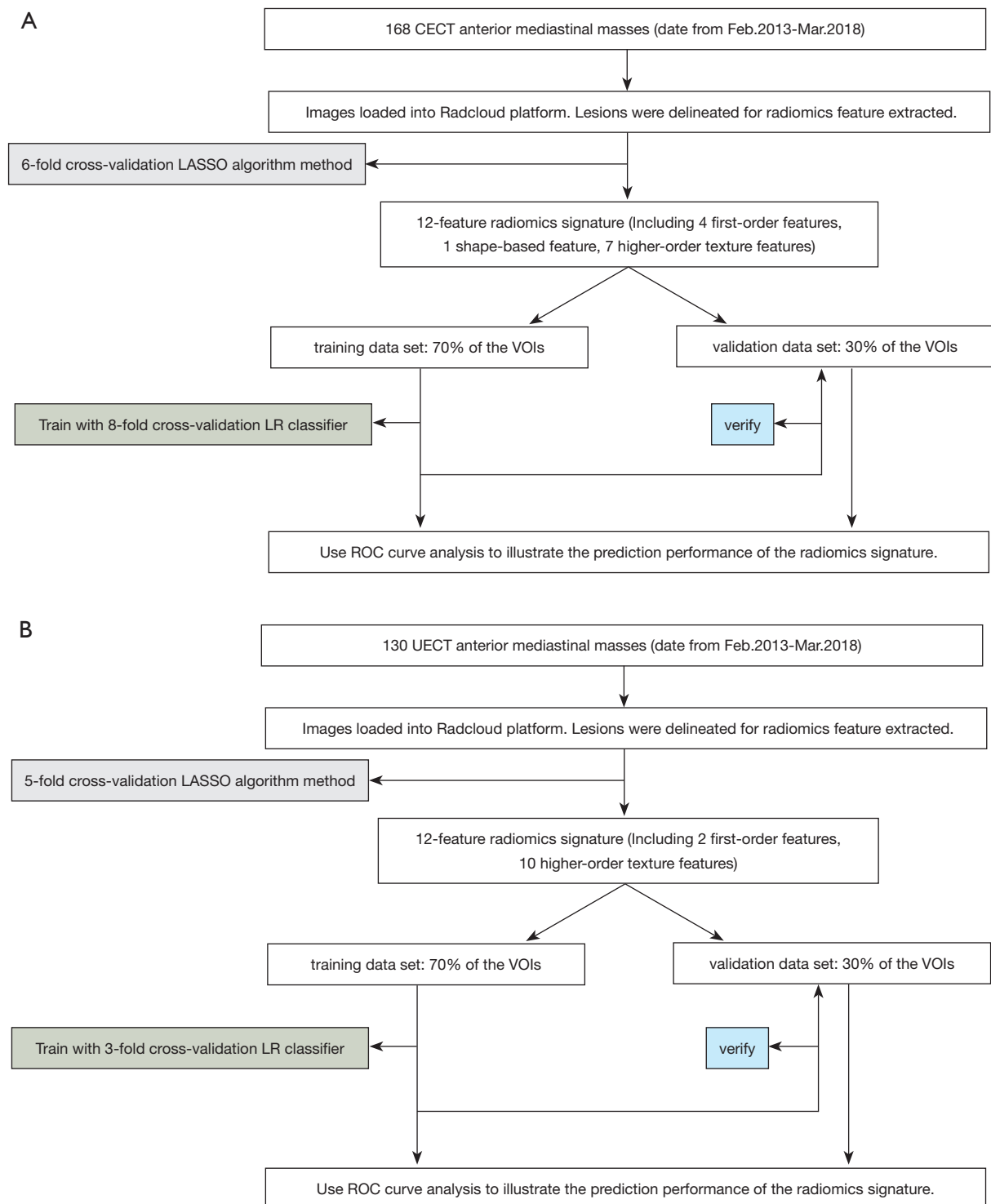


**Figure 2** Radiomics analysis workflow. First, the clinical UECT (A) and CECT (B) images of high- and low-risk anterior mediastinal lesions were collected. Second, image segmentation was used to delineate the anterior mediastinal lesions. Next, the image features were extracted by the automated high-throughput feature analysis algorithm. Finally, the statistical analysis was applied, and the sequential forward search was used for feature selection for the classification of anterior mediastinal lesions. UECT, unenhanced computed tomography; CECT, contrast-enhanced computed tomography.

**Table 2** Features of 12-radiomics models of UECT and CECT

Filters	Features
UECT	
Exponential	First order: mean
	Gray level non-uniformity
Wavelet	First order: 90 percentiles
	Cluster Prominence
	Gray level non-uniformity normalized
	Short run low gray level emphasis
	Cluster shade
	Small area low gray level emphasis
Square root	Long run low gray level emphasis
	Long run high gray level emphasis
	Zone variance
Square	Zone variance
CECT	
Shape	Spherical disproportion (shape)
Wavelet	First order: median
	First order: skewness
	Idn
	Size zone non-uniformity normalized
	Idmn
	Gray level non-uniformity normalized
Square	First order: kurtosis
	Small area low gray level emphasis
	Small area emphasis
Exponential	First order: total energy
	Zone variance

UECT, unenhanced computed tomography; CECT, contrast-enhanced computed tomography; Idn, inverse difference normalized; Idmn, inverse difference moment normalized.

## Results

### Clinical characteristics

A total of 298 patients (collected from February 2013 to March 2018) included 130 for UECT scan (28 high-risk lesions, 102 low-risk lesions; lesion volume,  $132.21 \pm 229.18$  and  $52.57 \pm 96.08$  cm<sup>3</sup>, respectively) and 168 for CECT scan (88 high-risk lesions, 90 low-risk lesions; lesion volume,

$128.85 \pm 227.17$  and  $53.14 \pm 96.45$  cm<sup>3</sup>, respectively). The differences in lesion volume between the high-risk and low-risk sets in UECT and CECT exhibited statistical significance ( $P=0.006$ ;  $P=0.009$ , respectively). Among the 130 patients of the UECT scan (59 males and 71 females; age range, 17–86 years old; mean,  $52.26 \pm 11.08$  years old) and the 168 patients for the CECT scan (72 men and 96 women; age range, 18–86 years old; mean,  $52 \pm 11.29$  years old), there was found to be no significant differences in age and gender between the high-risk and low-risk datasets ( $P=0.691$ ;  $P=0.082$  respectively).

### Radiomics features selection

Through the Lasso algorithm method, each of the UECT and CECT scans extracted 12 features, which displayed significant differences in distinguishing high-risk lesions from the low-risk ones in the anterior mediastinum, as shown in *Table 2*. Then, LR classifier was built using 12 features selected from Lasso process (*Figures 3,4*).

### Diagnostic performance of the radiomics model

The 12-feature model was trained with 8-fold and 3-fold cross-validation LR classifier in UECT and CECT respectively, with the ROC curve analysis results shown in *Figure 5* for UECT and in *Figure 6* for CECT. The AUC of the UECT training set was obtained as 0.842 (95% CI: 0.763–0.922; sensitivity 71.43%; specificity 74.07%); and the AUC of the UECT validation set was 0.774 (95% CI: 0.632–0.916; sensitivity 74.36%; specificity 72.73%). The AUC of the CECT training set and validation set were 0.741 (95% CI: 0.628–0.814; sensitivity 66.67%; specificity 64.81%), and 0.734 (95% CI: 0.597–0.872; sensitivity 62.96%; specificity 66.67%) respectively. This showed excellent predictive ability (*Table 3*).

## Discussion

This study built predicted models for UECT and CECT scans using LASSO with LR as the feature selection and classifier over the normalized radiomics features. The two 12-feature radiomics models showed good performances in distinguishing high-risk lesions from the low-risks in the anterior mediastinum, and the UECT scan was proven to outperform CECT regarding the prediction for risk evaluation.

There are a variety of tumors in the anterior mediastinum (thymomas, thymic carcinomas, thymic carcinoids,

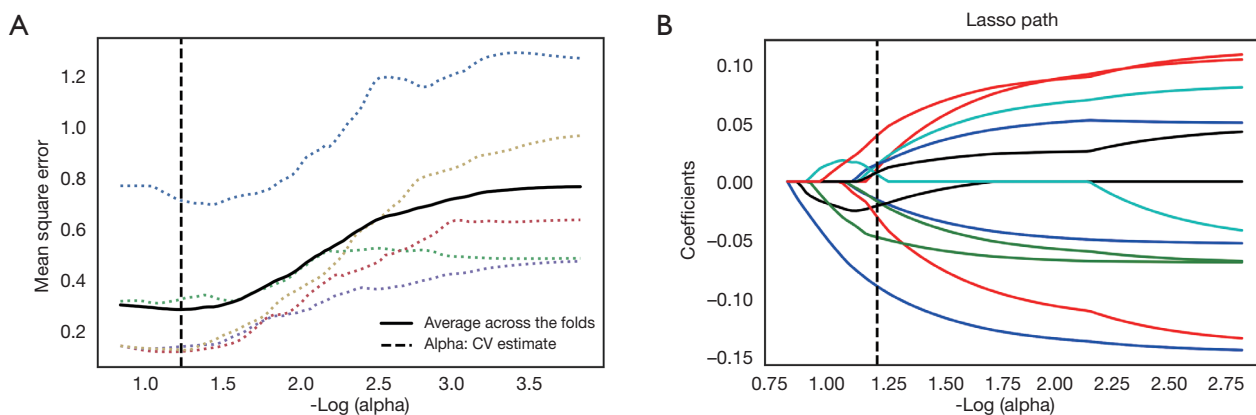


**Figure 3** Radiomics features selection of UECT using the LASSO regression. (A) Mean square error path diagram. The abscissa is log (alpha), and the dashed lines of different colors indicate that different features correspond to different alphas with different mean square errors; (B) LASSO path map, features corresponding to different alpha features. UECT, unenhanced computed tomography.

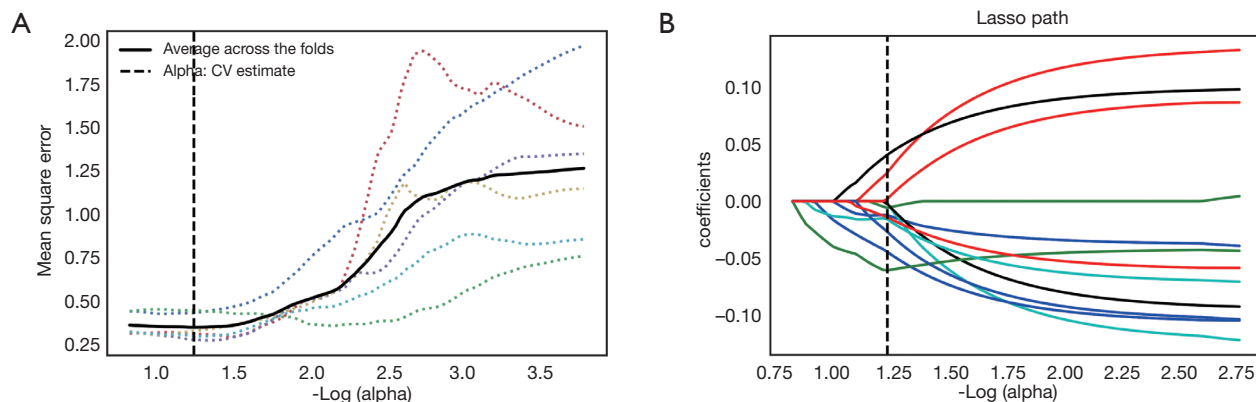


**Figure 4** Radiomics features selection of CECT using the LASSO regression. (A) Mean square error path diagram. The abscissa is log (alpha), and the dashed lines of different colors indicate that different features correspond to different alphas with different mean square errors; (B) LASSO path map, features corresponding to different alpha features. CECT, contrast-enhanced computed tomography.

lymphomas, germ cell tumors, lung metastases, etc.) or tumor-like lesions (intrathoracic goiter, thymic or bronchogenic cysts, lymphangiomas, aortic aneurysms, etc.) (3,17). Since surgical management differs for these conditions, it is essential to differentiate high-risk masses (including lymphomas, thymic carcinomas, WHO type B2, 3 thymomas and so on) from the low-risk ones (such as WHO types A, AB, B1 thymoma, thymic cysts, etc.) before treatment.

The invasive methods including biopsy, mediastinoscopy, and surgery are used in determining anterior mediastinum lesions routinely. Clinical follow-up is also a diagnostic way of determining anterior mediastinal lesions, but uncertain follow-up intervals may cause the widespread treatment

delay of high-risk lesions. The radiomics method introduced in this study was found to be helpful for diagnosing high-risk lesions in a timely manner without follow-ups and in avoiding invasive examinations. Characteristics of routine CT scans, such as lesion margin, enhancement, and surrounding tissue invasion, can help evaluate the risks in anterior mediastinum lesions. This method is limited by the professional aptitude of radiologists and suffers from inter-reader variability. Based on the recent investigation by Kong *et al.*, the value of the apparent diffusion coefficients (ADCs) is conducive to assessing the classification of thymic epithelial tumors (18). Although it eliminates subjective elements and acquires good diagnostic effects, MR is still not a routine examination and is not widely used in CT for

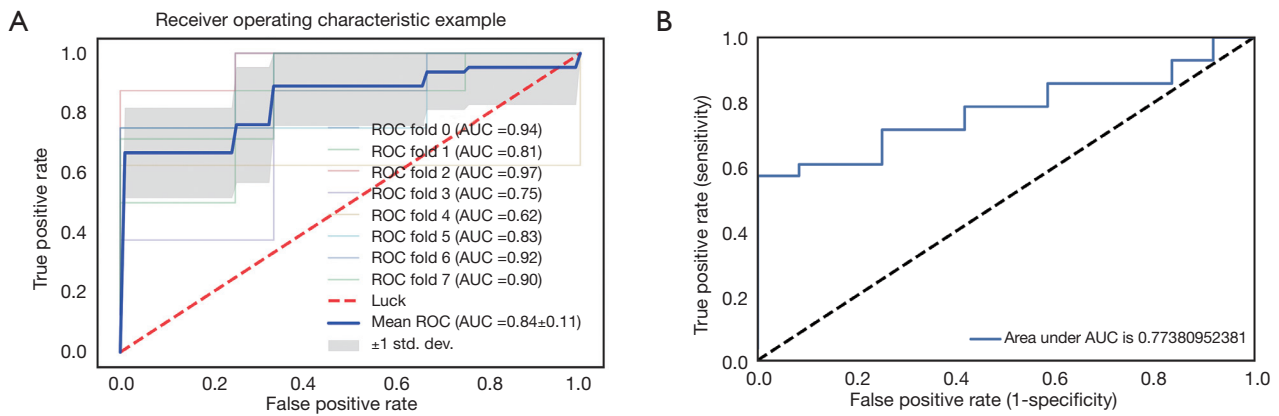


**Figure 5** Receiver operating characteristic curve on UECT. (A) The 12-feature model was trained in training set with 8-fold cross-validation LR classifier in UECT. The AUC was 0.842 (95% CI: 0.763–0.922; sensitivity 71.43%; specificity 74.07%); (B) the 12-feature model of The UECT validation set with the AUC of 0.774 (95% CI: 0.632–0.916; sensitivity 74.36%; specificity 72.73%). UECT, unenhanced computed tomography.

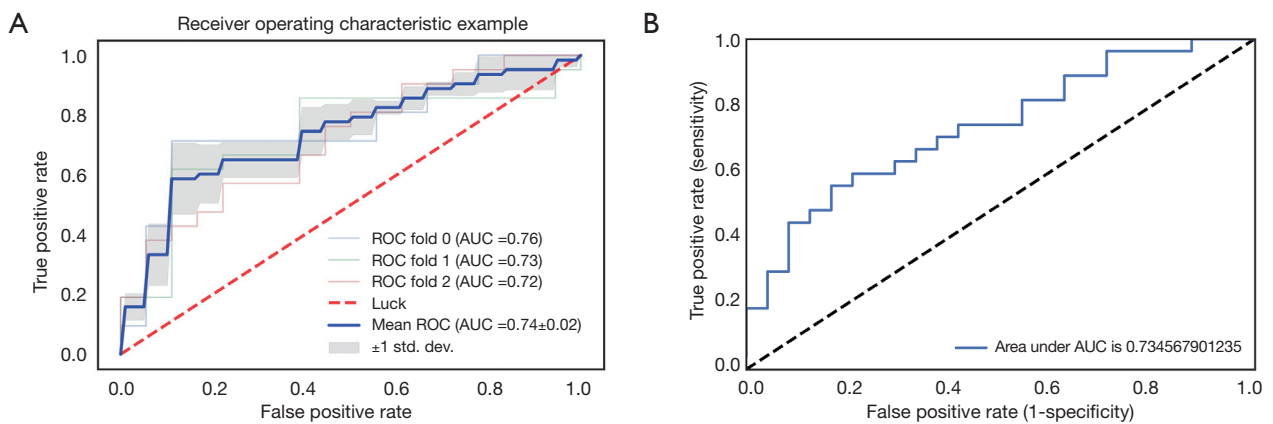


**Figure 6** Receiver operating characteristic curve on CECT. (A) The 12-feature model was trained in training set with 3-fold cross-validation LR classifier in UECT. The AUC was 0.741 (95% CI: 0.628–0.814; sensitivity 66.67%; specificity 64.81%); (B) the 12-feature model of The UECT validation set with the AUC of 0.734 (95% CI: 0.597–0.872; sensitivity 62.96%; specificity 66.67%). UECT, unenhanced computed tomography; CECT, contrast-enhanced computed tomography.

**Table 3** The risk classification performance of the radiomics models

Group	AUC	95%CI	Sensitivity (%)	Specificity (%)
UECT				
Training set	0.842	0.763–0.922	71.43	74.07
Validation set	0.774	0.632–0.916	74.36	72.73
CECT				
Training set	0.741	0.628–0.814	66.67	64.81
Validation set	0.734	0.597–0.872	62.96	66.67

UECT, unenhanced computed tomography; CECT, contrast-enhanced computed tomography; AUC, area under the curve.

anterior mediastinal lesions in clinical practice.

Some analyses have confirmed the distinguishing capability of the radiomic features for molecular subtypes and histologic grade in tumors, including gliomas (19), lung cancers (13), colorectal adenocarcinomas (20), bladder carcinomas (21), gastric cancer (22), prostate cancers (23), etc. In the glioma research (19), the AUC was between 0.922 and 0.975, and had an accuracy between 87.7% and 96.1% which was used to determine the histology and gradings of gliomas, providing a reliable alternative. Previous studies on anterior mediastinal masses are all based on QTA, which is a branch of radiomics category. In this study, both texture features and other categories of features were analyzed. In the two 12-feature radiomics models on UECT and CECT scans we obtained, 10 and 7 radiomics features, respectively, were from the texture feature group. When features of other categories were added, the predictions became more comprehensive. To increase the information content of extracted radiomics features, we delineated ROI along the lesion outline of every image, turning the ROIs into VOIs. Chaddad *et al.* (24) found that a 3D-wavelet transform could discriminate between colorectal cancer grades with the entropy feature, with higher accuracy and sensitivity than the two-dimensional (2D)-wavelet transform. The 3D analysis of whole lesions could be more representative of heterogeneity in tumors and offer a more complementary set of diagnostic information.

With no shape features in the 12-feature radiomics of UECT, one shape feature, shape-Spherical Disproportion, was selected from CECT, which might have been due to the enhancement scan highlighting the outline of the lesions. Since more texture features were selected from UECT than from CECT, the tumor heterogeneity was better detected in UECT, and the texture features from plain CT scan were found to be more significant in discriminating risk levels in anterior mediastinal lesions. In this study, high-risk lesions showed a larger size than low-risk ones, which was in line with the findings of Yanagawa *et al.*'s (25). Also, compared with CECT, UECT images showed higher accuracy, sensitivity, and specificity in distinguishing high-risk anterior mediastinal lesions. Since a large number of anterior mediastinal lesions were incidentally found on routine UECT, and hypersensitivity to iodinated contrast media was considered, it may be not necessary for CECT to perform further diagnosis.

Several limitations of this study are discussed as follows. First, two medical centers were enrolled, but the number of cases was still small. A multi-center collaboration is needed

to enlarge the sample size for reducing sample selection bias and regional differences. Second, it is hard to control the sampling errors produced among different CT machines. In addition, the manual sketching method for the image was laborious, time-consuming, and subjective; thus, a more effective and precise way to outline the image should be explored in further investigation.

## Conclusions

In conclusion, the CT radiomics model exhibited a strong correlation in differentiating high-risk lesions from low-risk lesions. This non-invasive method would be an economical way to perform early discrimination of high-risk anterior mediastinal lesions with an excellent diagnostic performance.

## Acknowledgments

None.

## Footnote

*Conflicts of Interest:* The authors have no conflicts of interest to declare.

*Ethical Statement:* This retrospective study received the approval from the Institutional Review Board (IRB number: 2019022607), and informed consent was obtained from all patients.

## References

1. Carter BW, Marom EM, Detterbeck FC. Approaching the patient with an anterior mediastinal mass: a guide for clinicians. *J Thorac Oncol* 2014;9:S102-9.
2. Suster S, Moran CA. Histologic classification of thymoma: the World Health Organization and beyond. *Hematol Oncol Clin North Am* 2008;22:381-92.
3. Marx A, Chan JK, Coindre JM, et al. The 2015 World Health Organization Classification of Tumors of the Thymus: Continuity and Changes. *J Thorac Oncol* 2015;10:1383-95.
4. Chen G, Marx A, Chen WH, et al. New WHO histologic classification predicts prognosis of thymic epithelial tumors: a clinicopathologic study of 200 thymoma cases from China. *Cancer* 2002;95:420-9.
5. Scorsetti M, Leo F, Trama A, et al. Thymoma and thymic carcinomas. *Crit Rev Oncol Hematol* 2016;99:332-50.

6. Strobel P, Bauer A, Puppe B, et al. Tumor recurrence and survival in patients treated for thymomas and thymic squamous cell carcinomas: a retrospective analysis. *J Clin Oncol* 2004;22:1501-9.
7. Abdel Razek AA, Khairy M, Nada N. Diffusion-weighted MR imaging in thymic epithelial tumors: correlation with World Health Organization classification and clinical staging. *Radiology* 2014;273:268-75.
8. Scorsetti M, Leo F, Trama A, et al. Thymoma and thymic carcinomas. *Crit Rev Oncol Hematol* 2016;99:332-50.
9. Carter BW, Okumura M, Detterbeck FC, et al. Approaching the patient with an anterior mediastinal mass: a guide for radiologists. *J Thorac Oncol* 2014;9:S110-8.
10. Lambin P, Rios-Velazquez E, Leijenaar R, et al. Radiomics: extracting more information from medical images using advanced feature analysis. *Eur J Cancer* 2012;48:441-6.
11. Kumar V, Gu Y, Basu S, et al. Radiomics: the process and the challenges. *Magn Reson Imaging* 2012;30:1234-48.
12. Gillies RJ, Kinahan PE, Hricak H. Radiomics: Images Are More than Pictures, They Are Data. *Radiology* 2016;278:563-77.
13. Song SH, Park H, Lee G, et al. Imaging Phenotyping Using Radiomics to Predict Micropapillary Pattern within Lung Adenocarcinoma. *J Thorac Oncol* 2017;12:624-32.
14. Iannarelli A, Sacconi B, Tomei F, et al. Analysis of CT features and quantitative texture analysis in patients with thymic tumors: correlation with grading and staging. *Radiol Med* 2018;123:345-50.
15. Yasaka K, Akai H, Abe O, et al. Quantitative computed tomography texture analyses for anterior mediastinal masses: Differentiation between solid masses and cysts. *Eur J Radiol* 2018;100:85-91.
16. Yasaka K, Akai H, Nojima M, et al. Quantitative computed tomography texture analysis for estimating histological subtypes of thymic epithelial tumors. *Eur J Radiol* 2017;92:84-92.
17. Strollo DC, Rosado de Christenson ML, Jett JR. Primary mediastinal tumors. Part 1: tumors of the anterior mediastinum. *Chest* 1997;112:511-22.
18. Kong LY, Zhang W, Zhou Y, et al. Histogram analysis of apparent diffusion coefficient maps for assessing thymic epithelial tumours: correlation with world health organization classification and clinical staging. *Br J Radiol* 2018;91:20170580.
19. Ditmer A, Zhang B, Shujaat T, et al. Diagnostic accuracy of MRI texture analysis for grading gliomas. *J Neurooncol* 2018;140:583-9.
20. Huang X, Cheng Z, Huang Y, et al. CT-based Radiomics Signature to Discriminate High-grade From Low-grade Colorectal Adenocarcinoma. *Acad Radiol* 2018;25:1285-97.
21. Xu X, Zhang X, Tian Q, et al. Quantitative Identification of Nonmuscle-Invasive and Muscle-Invasive Bladder Carcinomas: A Multiparametric MRI Radiomics Analysis. *J Magn Reson Imaging* 2019;49:1489-98.
22. Tang L. Radiological evaluation of advanced gastric cancer: from image to big data radiomics. *Zhonghua Wei Chang Wai Ke Za Zhi* 2018;21:1106-12.
23. Penzias G, Singanamalli A, Elliott R, et al. Identifying the morphologic basis for radiomic features in distinguishing different Gleason grades of prostate cancer on MRI: Preliminary findings. *PLoS One* 2018;13:e0200730.
24. Chaddad A, Daniel P, Niazi T. Radiomics Evaluation of Histological Heterogeneity Using Multiscale Textures Derived From 3D Wavelet Transformation of Multispectral Images. *Front Oncol* 2018;8:96.
25. Yanagawa M, Tomiyama N. Prediction of thymoma histology and stage by radiographic criteria. *Thorac Surg Clin* 2011;21:1-12, v.

**Cite this article as:** Sui H, Liu L, Li X, Zuo P, Cui J, Mo Z. CT-based radiomics features analysis for predicting the risk of anterior mediastinal lesions. *J Thorac Dis* 2019;11(5):1809-1818. doi: 10.21037/jtd.2019.05.32